Results in Physics 13 (2019) 102278

Contents lists available at ScienceDirect

Results in Physics

journal homepage: www.elsevier.com/locate/rinp

The physical properties of bismuth replacement in lead halogen perovskite solar cells: $CH_3NH_3Pb_{1-x}Bi_xI_3$ compounds by ab-*initio* calculations

C. Soykan[a,*], H. Gocmez[b]

[a] Vocational School of Health Services, Ahi Evran University, Kırşehir, Turkey
[b] Department of Metallurgy and Materials Engineering, Dumlupınar University, Kütahya, Turkey

A B S T R A C T

The selection of elements used in the design of solar cells is crucial in terms of environmental pollution and legalization problems due to the fact that both solar energy conversion efficiency as high as possible and toxic effects when dissolved in water. Hybrid Pb halogen solar cells demonstrate promising solar cell conversion material properties with a conversion rate of approximately 20%. However, Pb is a toxic element when dissolved in water. In this study, it was aimed to design new material forms for solar cells obtained by replacing Pb with a less toxic element without disrupting the photophysical properties of the material. This approach has been exemplified by focusing on bismuth considering Goldschmidt rules (GRs), Tolerance factor concept (*t*) and Shockley Queisser (SQ) limits. Non-stoichiometric $CH_3NH_3Pb_{(1-x)}Bi_{(x)}I_3$ crystal structure were formed at the ratios determined by x = 0.125, 0.25, 0.75 and 1.00 values by replacing Bi^{3+} with Pb^{2+}. Using the Density Functional Theory (DFT), the effect of added Bismuth ions in the structural and electronic properties of the material was investigated. According to the Shockley Quisser (SQ) limit, the crystal form $CH_3NH_3Pb_{0.875}Bi_{0.125}I_3$ formed with x = 0.125 ratio was determined to be the most suitable structure in terms of solar cell productivity with a direct band gap of 1.30 eV. In addition, the band gaps of $CH_3NH_3Pb_{0.500}Bi_{0.500}I_3$ and $CH_3NH_3Pb_{0.250}Bi_{0.750}I_3$ formed at x = 0.50 and 0.75 were calculated to be 1.0863 eV and 1.0895 eV, respectively. Band gaps of these phases were also within the SQ limit. However, the band gap of the $CH_3NH_3PbI_3$ stoichiometric phase was calculated to be 1.6826 eV above the SQ limit, while the $CH_3NH_3BiI_3$ phase band gap was calculated to be 0.2738 eV well below the SQ limit. According to our DFT calculations, organic halogen perovskite compounds in the form of $CH_3NH_3Pb_{(1-x)}Bi_{(x)}I_3$ formed at ratios of x = 0.125, 0.50 and 0.75 have been found to be more efficient than $CH_3NH_3PbI_3$ compounds in terms of solar energy conversion capacity, optoelectronic systems and environmental safety.

Introduction

Inorganic and organic hybrid perovskite solar cells are notable for their high power conversion efficiencies and low production costs. It has being studied to improve the electronic and optical properties of such solar cells. The dependence of the $CH_3NH_3^+PbX_3^-$ ($X = CI, Br, I$) crystal structure on the temperature was investigated by Poglitsch and Weber with x-ray diffraction [1]. The $CH_3NH_3^+PbI_3^-$ structure was found to have a tetragonal crystal structure with space group I4/m or I4/mcm at room temperature and a cubic phase transformation was observed at $T_c = 327.4$ K [1]. It was found a phase transformation from the tetragonal to orthorhombic symmetry (space group $Pna2_1$), which shows that a central symmetric unit cell passes through a central non-symmetric unit cell [1]. This transition can cause the material to have ferroelectric and antiferroelectric properties. Thus, it is likely that the electronic properties of the material, such as the band gap, will change. The electronic and optical properties of $CH_3NH_3PbI_3$, $CH_3NH_3PbI_3BF_4$, $CH_3NH_3PbI(BF_4)_2$ and $CH_3NH_3PbI(BF_4)_2$ perovskite phases were investigated using the first principles method by Rani and Singh based on Density Functional Theory (DFT) [2]. In the study of Rani, the band gap of $CH_3NH_3PbI_3$ crystal form are calculated as 1.73 eV. The configuration for solar cell of the perovskite $CH_3NH_3Pb_{1-x}Sb_xI_3$ (x = 0 ve 0.15) crystal structure by using Rietveld treatment technique are studied by Ando and et al. [3]. When Ando's results are examined, the addition of Sb atoms with a smaller atomic radius instead of Pb atoms reduces the lattice constant of the material. This effect also results in the expansion of the band gap. Mosconi et al. [4] have been indicated that organometal $CH_3NH_3PbX_3$ and mixed halide $CH_3NH_3PbI_2X$ (X = CI, Br, I) perovskite materials are important for highly productive solid-state cells. It is also stated that the interaction of the organic and inorganic components mediated by the hydrogen bond between the ammonium and halide groups in the work plays an important role on the structural variability of the material [4]. Kojima et al. [5] have focused on the Pb halide perovskite $CH_3NH_3PbBr_3$ and $CH_3NH_3PbI_3$ compounds for visible light sensitizing functions in photoelectrochemical cells. They reported that $CH_3NH_3PbI_3$ based cells can convert solar energy to 3.8% efficiency and a high photovoltage yield of 0.96 V. Saffari et al. [6] have investigated the structural and optical properties of chlorine doped non-stoichiometric $CH_3NH_3PbI_{3-x}CI_x$ (x = 0, 1, 2, 3) perovskite cubic phase by using DFT method. By using the data obtained here, they have studied properties such as light absorption efficiency and single-juk optical current density. The results

* Corresponding author.
E-mail address: cengiz.soykan@ahievran.edu.tr (C. Soykan).

https://doi.org/10.1016/j.rinp.2019.102278
Received 24 January 2019; Received in revised form 2 April 2019; Accepted 6 April 2019
Available online 13 April 2019
2211-3797/ © 2019 The Authors. Published by Elsevier B.V. This is an open access article under the CC BY-NC-ND license (http://creativecommons.org/licenses/BY-NC-ND/4.0/).

show that when chlorine is doped, the band gap increases; the lattice constants, the optical properties such as reactive index and damping coefficient decrease. Although organic Pb halogen perovskite compounds are an important material in terms of conversion efficiency of solar energy, a solar cell technology based on water-soluble Pb seems to be disadvantages due to environmental pollution and legalization problems. For this reason, it is important to investigate materials with good photoelectric properties by using less toxic elements instead of Pb. Jacobsson et al. [7] have investigated other metal ions that could be replaced in place of Pb, adhering to the Goldschmidt (GRs) rules and also taking into account the quantum mechanics . Sr^{2+} ion, whose ionic radius is almost the same as Pb^{2+}, was used. Strontium is a relatively inexpensive and non-toxic element. However, the band gap of $CH_3NH_3SrI_3$ was calculated to be 3.6 eV, which was too high for efficient photo-absorption. This study only revealed $CH_3NH_3SrI_3$ perovskite crystal structure [7]. Recently, it has worked on modeling Bismuth addition to $CH_3NH_3PbI_3$ perovskite structure using first-principle methods by Mosconi and et al. [8]. It has been reported that heterovalent Bi doping to the perovskite structures was limited in terms of efficiency and the doped Bi^{3+} ions acted as a deep electron trap. The details of the Goldschmidt empirical replacement rules (GRs) used in studies based on the element displacement approach are also given in Goldschmidt's study on the laws of crystal chemistry [9].

There are some physical limits in the crystal structures when the photoelectric converter solar cells are produced. First, the use of toxic elements in water-soluble cells causes environmental pollution and legalization problems. Second, although the doping of non-toxic elements instead of Pb seems to be a solution, limitations such as the Shockley Queisser limit and the Goldschmidt tolerance factor determine the number of elements that can be used. In addition, the value of the band gap of the material to be used for the ideal conversion efficiency is also very important. $CH_3NH_3PbI_3$ perovskite crystal form consists of $CH_3NH_3^+$ organic group (A cation), Pb^{2+} cation (B cation) and halogen I^- anion (C anion). The crystal ionic radius of $CH_3NH_3^+$ organic cation is 0.180 nm, for Pb^{2+} it is 0.132 nm and for I^- it is 0.206 nm [10]. The crystal ionic radius of Bi^{3+} is given as 0.117 nm [11]. In this study, according to x = 0.125, 0.25, 0.50, 0.75 and 1.00 ratios, non-stoichiometric $CH_3NH_3Pb_{(1-x)}Bi_{(x)}I_3$ forms are constructed by doping Bi^{3+} instead of Pb^{2+}. Using the Goldschmidt rules, Shockley Queisser limit, quantum mechanical approach and DFT calculation techniques, it is aimed to investigate photophysics of metal halogen perovskites and to determine the structural and electronic properties of the new hybrid solar cells by examining the contribution of promising Bi^{3+} instead of Pb^{2+}. In addition, to the best of our knowledge, no detailed theoretical or experimental data concerning non-stoichiometric $CH_3NH_3Pb_{(1-x)}Bi_{(x)}I_3$ perovskites for x values from 0.125 to 1.00 have been reported in the literature.

Computational method

In this study, ab-initio simulation calculations based on the Density Functional Theory (DFT) were performed using the potential of the projector augmented wave (PAW) to solve the Kohn-Sham equations [12–14]. Total energy calculations were performed using the Vienna ab-initio simulation package (VASP) [15–19]. The effects of electronic exchange and correlation functions were considered using the Generalized Gradient Approximation (GGA) developed by Burke, Perdew and Ernzerhof [20]. In our calculations, kinetic energy cutoff value for $CH_3NH_3PbI_3$ crystal phase was determined to be 600 eV. The energy convergence criterion of the electronic self-consistency was chosen as 10^{-8} eV/atom [21]. In the non-stoichiometric $CH_3NH_3Pb_{(1-x)}Bi_{(x)}I_3$ phases, a kinetic energy cut-off value of 500 eV and convergence value 10^{-8} eV/atom were used. The Brillouin zone integrations were carried out by Monkhorst-Pack special points mesh with a grid size of 12x12x12 (for $CH_3NH_3PbI_3$ and $CH_3NH_3BiI_3$) and 6x6x6 (for martensitic $CH_3NH_3Pb_{(1-x)}Bi_{(x)}I_3$) [22]. The contribution of valence electrons is influential in determining the electronic properties of material. The valence electron configurations for C, N, H, Pb, Bi and I atoms are $2s^2 2p^2$, $2s^2 2p^3$, $1s^1$, $5d^{10} 6s^2 6p^2$, $5d^{10} 6s^2 6p^3$ and $5s^2 5p^5$, respectively. Generally known, geometric optimization calculations have been made to determine the equilibrium state with the smallest energy. To determine the electronic behavior of the material, the density of states (DOS) was calculated using the tetrahedron method involving Bloch corrections. In addition, partial density of states (pDOS) calculations have been carried out to examine in more detail the contributions of the Pb, Bi and I atoms to the electron density of the material. The cubic $CH_3NH_3PbI_3$ crystal lattice was iterated by 2x2x2 ratio and transformed into super-lattice. Bi^{3+} ions instead of Pb^{2+} ions were placed according to x values to form non-stoichiometric $CH_3NH_3Pb_{(1-x)}Bi_{(x)}I_3$ crystal phases. As a result of Sr, CI, Br, Co, Ca and Bi substitutions to the perovskite crystal structure, studies have been focused on the changes in the physical properties of the structures. On the other hand, among these atoms, it was particularly focused on the dopant of Bi^{3+} ion [23–28]. Besides, The difference between the ionic radius of Bi^{3+} and the ionic radius of Pb^{2+} is about 11.36%. Since this value is less than 15%, it can be said that a full compliance can be achieved in terms of Goldschmidt's empirical substitution rules. In addition, the Bi^{3+} and Pb^{2+} cations are isoelectronic ($6s^2$) and have similar chemical properties [11]. Bi^{3+} has a stable oxidation state of + 3. Since it has similar ionic radius and electronic structure with Pb^{2+}, it can be expected to be similar in optoelectronic properties [29]. Since the Bi^{3+} ion has a similar ionic radius as Pb^{2+}, it is expected to substitute the position of the Pb^{2+} ions in the perovskite crystal structure. However, Mosconi et al. [8] reported that the doped Bi^{3+} ions behavior as a deep electron trap. On the other hand, it has been shown by Snaith et al. [28] that the color change seen in the Bi-doped $CH_3NH_3PbI_3$ crystal occurs due to increased defect states and to increase in the sub-band gap density of states.

In our calculations, there are 12 atoms in $CH_3NH_3PbI_3$ crystal phase and 50 valence electrons (read from the POTCAR file) in total. Similarly, in the $CH_3NH_3BiI_3$ phase there are also 12 atoms and 51 valence electrons (read from the POTCAR file). The same approach was also used in the calculation of non-stoichiometric crystal structures. At the beginning of our stoichiometric and non-stoichiometric calculations for heterovalent doping, we used the “nelect” parameter to consider the change in the total number of valence electrons of the crystal structures due to the addition of Bi^{3+} ion. It should not be forgotten that, as is known, with the vasp code only the total number of valence electrons of the system can be controlled. In addition, the vasp code will automatically add a background jellium to make the supercell in neutral charge and the jellium charge is distributed in the volume [15–19]. The calculations were first initiated from the cubic $CH_3NH_3PbI_3$ crystal phase, which had a stoichiometric 12 atom (containing C 1, N 1, H 6, Pb 1 and I 3 atoms). Space group of cubic crystal structure of $CH_3NH_3PbI_3$ is space group 221 ($Pm\bar{3}m$, $Pm\bar{3}m$ or $Im\bar{3}m$). The position of atoms in crystal structure is given by C (0.896, 0.999, 0988), N (0.142, 0.999, 0,032), H (0.866, 0.999, 0.805; 0.822, 0.152, 0.064; 0.822, 0.847, 0.065; 0.221, 0.142, 0.965; 0.221, 0.856,0.965; 0.180, 0.999, 0.205), Pb (0.475, 0.500, 0.477) and I (0.428, 0.499, 0.972; 0.433, 0.000, 0.512; 0.967, 0.500, 0.439), respectively. After the crystal lattice was relaxed, the electronic density of state (DOS) and partial density of state (pDOS) were calculated. Stoichiometric unit cells containing 1 Pb and 1Bi atoms are given in Fig. 1. In the second step, the relaxation and electronic state densities (DOS and pDOS) of the non-stoichiometric $CH_3NH_3Pb_{(1-x)}Bi_{(x)}I_3$ structure were calculated. Super-lattice of non-stoichiometric crystal structures are given also in Fig. 2a)–d), respectively. Crystal structure of nonstoichiometric phases were obtained by using initial cubic structure of CH3NH3PbI3 that is created with extension by 2x2x2 through ×, y and z directions. After Bi atoms were positioned at proper location in the structure, the obtained new phase was relaxed until the defined conditions were reached. This calculation

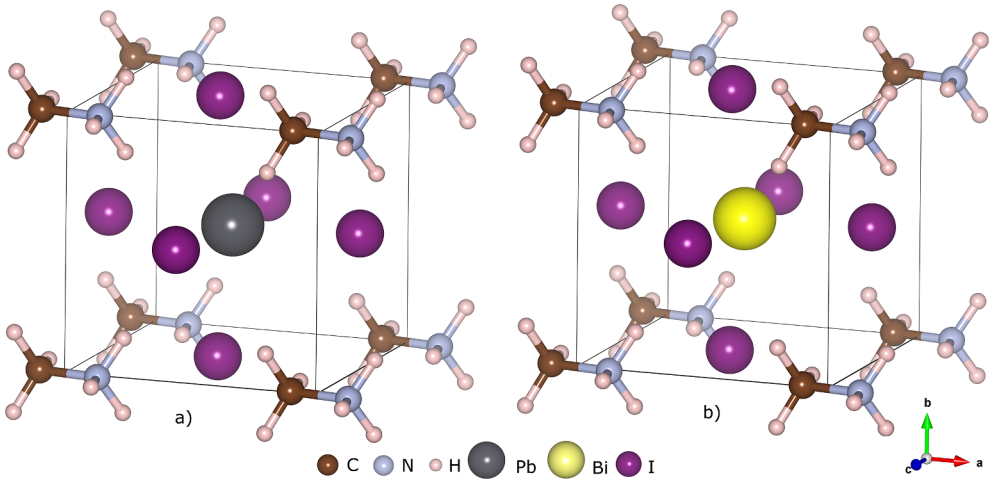

Fig. 1. a) $CH_3NH_3PbI_3$ and b) $CH_3NH_3BiI_3$ perovskite cubic and orthorhombic phases unit cell crystal structures. Brown, gray, cream, black, yellow and purple circles in the pictures represent C, N, H, Pb, Bi and I atoms, respectively. (For interpretation of the references to color in this figure legend, the reader is referred to the web version of this article.)

reveals that final relaxed and stable crystals phase has orthorhombic structure with space group 33 (Pna21)

The concept of tolerance factor (t) for perovskite structures should be considered in order to examine process of the placement of Bi^{3+} ion instead of Pb^{2+} cation at x = 0.125, 0.25, 0.50, 0.75 ratios in organic halogen perovskite material in terms of Goldschmidt's rules. The tolerance factor, t, with respect to the ionic radius of the actual ions is given as follows:

$$t = \frac{r_A + r_C}{\sqrt{2}\,(r_B + r_C)} \tag{1}$$

where r_A, r_B ve r_C are the ionic radius of the A, B and C ions,respectively. It has been reported that; If the value of the tolerance factor t is $0.7 < t$ less than 0.9, the crystal structure is tetragonal, orthorhombic or rhombohedral (the A cation can be too small or the B cation can be very large); If $0.9 < t$ less than 1.0, the crystal structure can be cubic crystal phase (ideal perovskite crystal structure); if $t > 1.0$; the

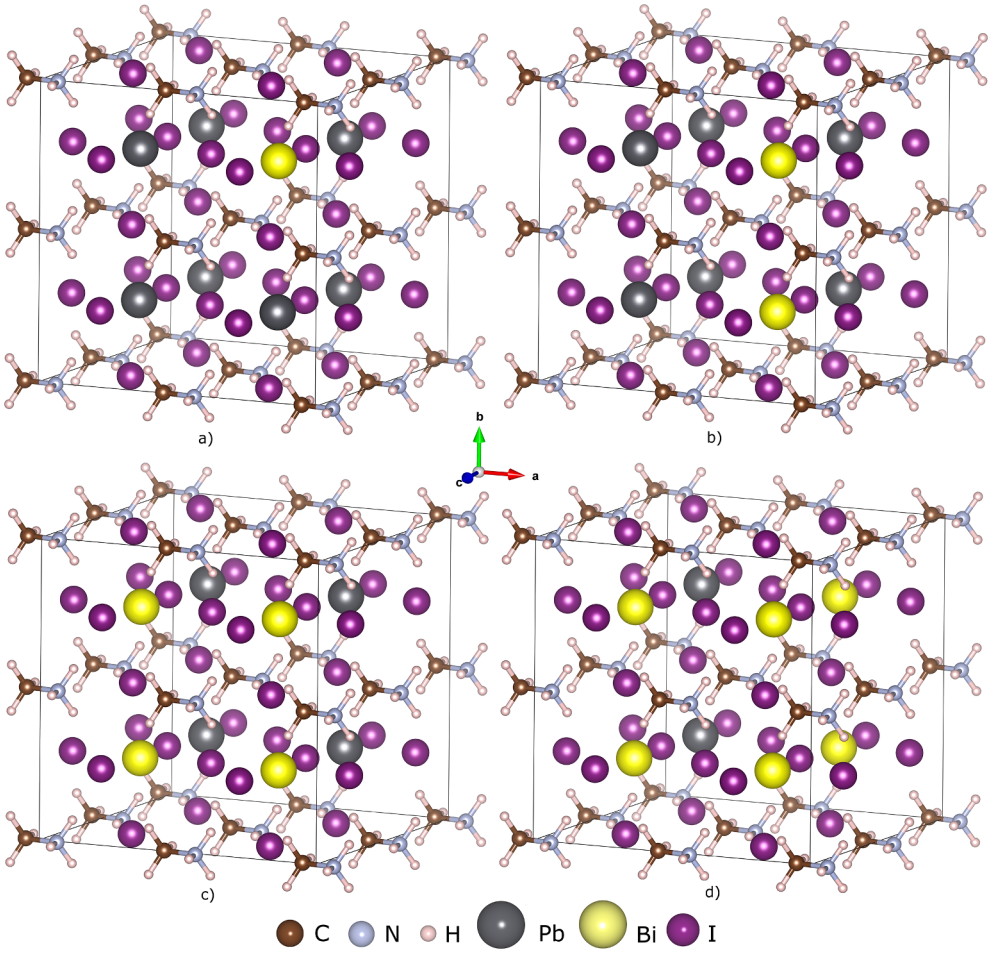

Fig. 2. The super cell crystal structures of $CH_3NH_3Pb_{(1-x)}Bi_xI_3$ perovskite phases are designed by x ratio a) 0.125, b) 0.25, c) 0.50 and d) 0.75, respectively. Brown, gray, cream, black, yellow and purple circles in the pictures represent C, N, H, Pb, Bi and I atoms, respectively. (For interpretation of the references to color in this figure legend, the reader is referred to the web version of this article.)

Table 1
The lattice constants of the stoichiometric $CH_3NH_3PbI_3$ and $CH_3NH_3BiI_3$ crystal structures and the other theoretical and experimental data.

Structure	Method	Lattice Constants (A^0)			Ref.
		a	*b*	*c*	
$CH_3NH_3PbI_3$	our cal.	6.406	6.406	6.406	
	other cal.	6.420	6.420	6.420	[2]
		6.330	6.330	6.330	[4]
		6.310	6.310	6.320	[6]
		6.172	6.149	6.218	[33]
	exp.	6.328	6.328	6.328	[1]
		6.288	6.288	6.288	[3]
		6.180	6.180	6.180	[34]
$CH_3NH_3BiI_3$	our cal.	6.967	6.064	6.155	

crystal structure be multi-layered crystal phases (A cation can be too large) [30,31,32]. According to Eq. (1), the tolerance factor (*t*) was calculated to be 0.85 for the crystal structure acquired from the addition of Bi^{3+} ion in place of the Pb^{2+}. The 0.85 value indicates that the perovskite is not cubic at room temperature, while obtained crystal structure is very close to the ideal perovskite cubic boundary. The empirical rules for element substitution with respect to Goldschmidt, if the ionic radius differs by less than 15%, a full perfectly substitution can occur, but, if the size differs between 15 and 30%, limited substitution can occur. Thus, the charge of the material changes and the charge neutrality is restored by changing the charges of the other elements [9]. The difference between the ionic radius (0.117 nm) of Bi^{3+} and the ionic radius (0.132 nm) of Pb^{2+} is approximately 11.36%. This difference, according to Goldshmidt's empirical substitution rules, is less than 15%, indicating that substitution can easily occur. As a result of our calculations, as given in Tables 1 and 2, the stoichiometric and non-stoichiometric perovskite structures are transformed to the orthorhombic crystal form when by added Bi^{3+} ions with respect to x ratio. The transition of stable crystal phases to orthorhombic symmetry corresponding to the minimum energy reached as a result of the simulation is a consequence of methylammonium cations not having a spherical symmetry.

Results and discussion

Structural properties of stoichiometric phases

$CH_3NH_3PbI_3$ perovskite material has been reported by previous theoretical [4,7,33] and experimental [3,34,35] studies in which the cubic (Pm3m), tetragonal (I4/mcm) and orthorhombic (Pna21) crystal phases were defined. In this study, the structural and electronic properties of the $CH_3NH_3PbI_3$ crystal form were calculated. There are 1C, 1 N, 6H, 1 Pb and 3 I atoms in $CH_3NH_3PbI_3$ given in Fig. 1a) unit cell with 12 atom. As given in Fig. 1b) the $CH_3NH_3BiI_3$ crystal form with 12 atoms are obtained by doping Bi^{3+} ions instead of Pb^{2+} ions.

In our calculations, the lattice constant of the cubic phase of $CH_3NH_3PbI_3$ was calculated as $6.406A^0$ with a unit cell volume of $262.88A^3$. The calculated lattice constant is consistent with the theoretical data in the range of from $6.172A^0$ to $6.420A^0$ [2,4,6,33] and also the experimental lattice constants varying between $6.180A^0$and $6.288A^0$ [1,3,34]. The lattice constant calculated as $6.406A^0$ differs 2–3% ratio deviation from the experimental data. The lattice constants of $CH_3NH_3BiI_3$ phase are also calculated as $6.967A^0$, $6.064A^0$ and$6.155A^0$. The lattice constants of the $CH_3NH_3BiI_3$ crystal formed by the addition of 1 mol of Bi^{3+} ion instead of 1 mol of Pb2 + were estimated to be about 9%, 5% and 4% deviation ratio from the cubic phase, respectively. Our results are presented in Table 1 for comparison with other experimental and theoretical studies.

Structural properties of Non-stoichiometric phases

The crystal structure of $CH_3NH_3PbI_3$ given in Fig. 1a) was selected as the initial phase and x = 0.125 was taken to form the first non-stoichiometric $CH_3NH_3Pb_{(1-x)}Bi_{(x)}I_3$ structure. The crystal lattice was shifted to 2x2x2 (containing C 8, N 8, H 48, Pb 7, Bi 1 and I 24 atoms) have been obtained the $CH_3NH_3Pb_{0.75}Bi_{0.25}I_3$ supercell. This supercell is given in Fig. 2a).

Similarly, x = 0.25, 0.50 and 0.75 were selected to obtain $CH_3NH_3Pb_{0.750}Bi_{0.250}I_3$, $CH_3NH_3Pb_{0.500}Bi_{0.500}I_3$ and $CH_3NH_3Pb_{0.250}Bi_{0.750}I_3$, respectively. Supercells of these phases are presented in Fig. 2b)–d), respectively.

In the geometric optimization calculations, the structural properties of the crystal phases in the equilibrium state are calculated when the external pressure applied to the crystal is about 0 kbar and the total force applied on each atom reaches about$0.01eV/A^0$. The results obtained are listed in Table 2.

Based on the varying x values from 0.125 to 0.75, it was determined that the addition Bi^{3+} ions instead of Pb^{2+} ions did not alter the crystal lattice constants and the angles between the ×, y, and z directions. However, the lattice constants calculated for the non-stoichiometric $CH_3NH_3Pb_{(1-x)}Bi_xI_3$ phases deviate 0.6%, 0.008% and 1.38% ratios, respectively, from the lattice constant of the initial phase $CH_3NH_3PbI_3$ ($6.406A^0$). It is seen that the crystal structures of the non-stoichiometric phases are transformed from the cubic phase to orthorhombic phase, while the deviation rates in the lattice constants are very small. This result supports the crystal form (orthorhombic) predicted by the value of the tolerance factor calculated as 0.85 for the added Bi^{3+} ions crystal phase depending on the x values.

Electronic properties of stoichiometric phases

The total electron state density (DOS) of the stoichiometric $CH_3NH_3PbI_3$ and $CH_3NH_3BiI_3$ phases and the partial (pDOS), which describes the contributions from the individual electronic states, are shown in Fig. 3a) and b), respectively. The Fermi level is shifted to 0 eV in the all figures. When examining the electronic properties of the $CH_3NH_3PbI_3$ structure given in Fig. 3a), the lowest valence bands around −8 eV are predominantly due to the states 6 s-6p and 5d of the Pb atoms. The valence band between −3 eV and the Fermi level predominantly consists of the 5 s and 5p states of the I atoms. In the conduction band distributed between 2 eV and 6 eV, especially the states s, p and d of the Pb atoms dominate in the contributions coming

Table 2
The calculated lattice constants of non-stoichiometric crystal structures of $CH_3NH_3Pb_{(1-x)}Bi_xI_3$ perovskite phases are designed by x ratio a) 0.125, b) 0.25, c) 0.50 and d) 0.75, respectively.

Structure	x ratio	Lattice constants (A^0)			Angles between ×, y, and z directions		
		a	*b*	*c*	*α*	*β*	*γ*
$CH_3NH_3Pb_{0.875}Bi_{0.125}I_3$	0.125	6.443	6.406	6.494	90.024	89.841	90.019
$CH_3NH_3Pb_{0.750}Bi_{0.250}I_3$	0.250	6.443	6.406	6.494	90.024	89.841	90.019
$CH_3NH_3Pb_{0.500}Bi_{0.500}I_3$	0.500	6.443	6.406	6.494	90.024	89.841	90.019
$CH_3NH_3Pb_{0.250}Bi_{0.750}I_3$	0.750	6.443	6.406	6.494	90.024	89.841	90.019

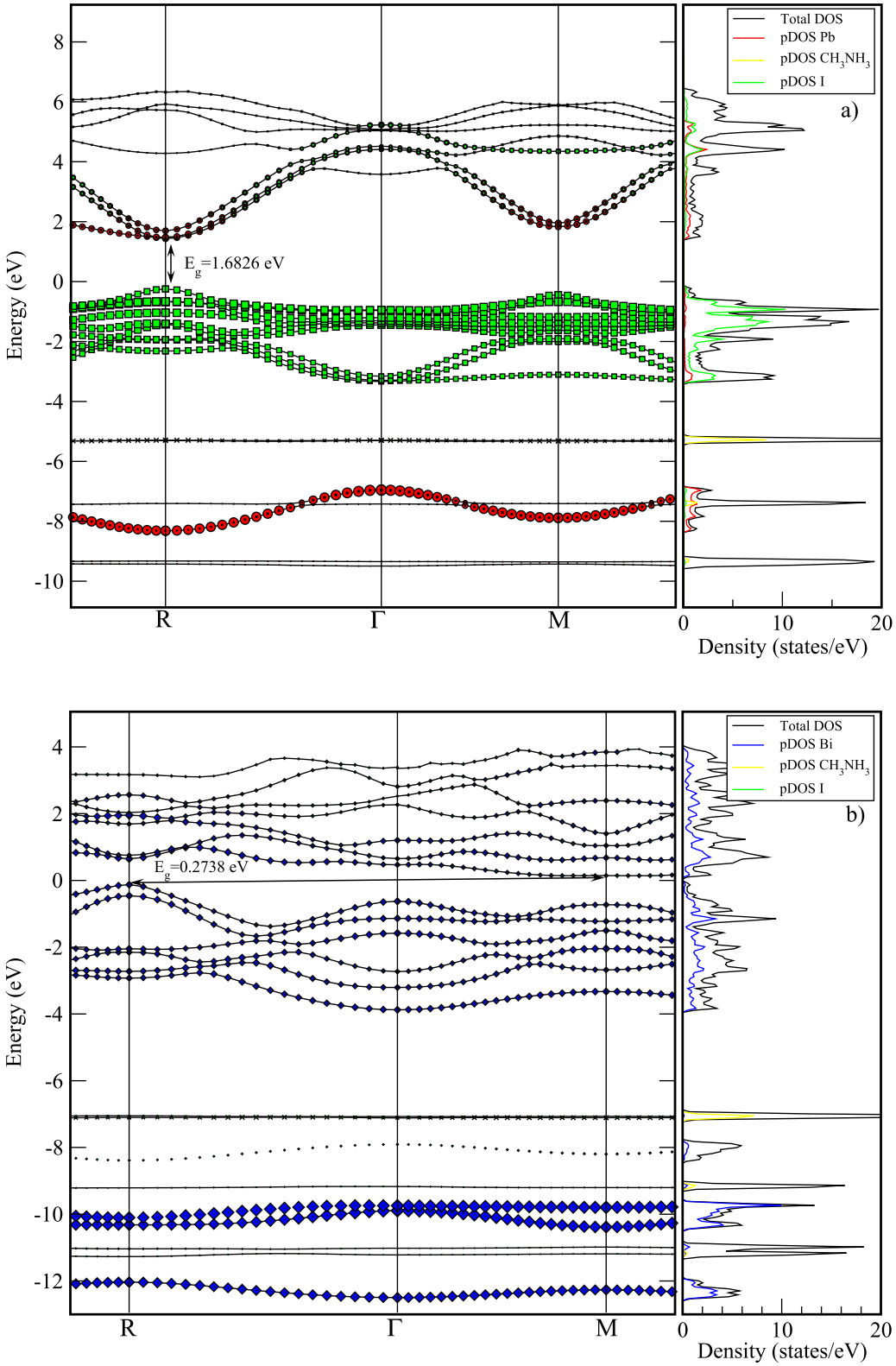

Fig. 3. The calculated band structures of the stoichiometric a) $CH_3NH_3PbI_3$ and b) $CH_3NH_3BiI_3$ phases in the direction $F \rightarrow R \rightarrow \Gamma \rightarrow M \rightarrow \Gamma \rightarrow F$. In order to increase the resolution, the $R \rightarrow \Gamma \rightarrow M$ line is zoomed. The fermi level is at 0 eV.

to the lower parts of the band. In the 3 eV and higher parts, contributions of both Pb and I atoms have been observed. The top part of the valence band is at −0.246 eV and the bottom part of the conduction band is at 1.4362 eV. In the R symmetry point, the presence of both the top part of the valence band and the bottom part of the conduction band indicates that the cubic $CH_3NH_3PbI_3$ phase has an electronic direct band gap. The band gap are calculated as 1.6826 eV. The obtained results are given in Table 3 for comparison with other studies. The calculated band gap in this study is compatible with both theoretical and experimental studies. However, it shows a deviation of at least 3%

Table 3
The calculated band gaps of the stoichiometric $CH_3NH_3PbI_3$ and $CH_3NH_3BiI_3$ crystal structures and the other theoretical and experimental data.

Structure	Method	Band gap	Ref.
		$E_{band-gap}(eV)$	
$CH_3NH_3PbI_3$	our cal.	1.682	
	other cal.	1.730	[2]
		1.570	[4]
		1.500	[6]
		1.600	[7]
		1.530	[8]
		1.810	[33]
	exp.	1.550	[5]
		1.550	[35]
		1.610–1.680	[36]
		1.600	[37]
		1.550	[38]
$CH_3NH_3BiI_3$	our cal.	0.274	

and at most 11% from the theoretical studies. In terms of experimental studies, it was very consistent with the value given in [36], but deviated by 8% from other studies.

Fig. 3b) shows the electronic band distribution of the $CH_3NH_3BiI_3$ phase. In both the valence-conduction bands and the high-low energy regions, the contributions in the 6 s- 6p and 5d states of the Bi atoms are rather dominant over the contributions from the other atoms. However, the highest level of the valence band is at the R symmetry point of −0.128 eV, while the lowest level of the conduction band is at the M symmetry point of 0.1451 eV. Thus, the energy band gap of the $CH_3NH_3BiI_3$ phase was calculated to be a very small value of 0.2738 eV. Due to the top point of the valence band and the bottom point of the conduction band are located at different symmetry points (R and M), it is seen that the $CH_3NH_3BiI_3$ phase has an electronic indirect band gap. When Fig. 3a) and b) are examined, while the peak of the valence band maintains a value of −0.128 eV, the lowest level of the conduction band decreases from 1.4362 eV to 0.1451 eV. As a result of this change, a narrower band gap is formed. For the perovskite structures in the $A-B-C_3$ general form, the electronegativity of the B cation was reported to be more effective on the band width than the A cation [39,40]. Accordingly, reducing the electronegativity of B cation will increase the band gap of the material. In addition, the character of the $B-C$ bond is also effective on band width and the increase in the antibonding character of the $B-C$ bond will also result in an increase in band gap [39]. Differences in orbit symmetries are a source of these effects and can lead to the possibility of different hybridizations. The electronegativity of Bi, Pb and I elements are given as 2.02, 2.33 and 2.66, respectively. Bismuth's electronegativity is relatively smaller than the electronegativity of lead. This would increase the antibonding character of the $Bi-I$ bonds by some amount relative to the $Pb-I$ bonds. While it was expected that the increase of the antibonding effect between the anion and the cation would increase the band gap, In our calculations, it was determined that the band gap by displacement of the Bi^{3+} ions is decreased due to approach of the conduction band to the valence band. In order to be able to explain this effect, it is necessary to focus on two physical properties. First, the difference between electronegativity of Bi, Pb and I elements is rather small. This little difference in electronegativity ensures that the change of antibonding character is very small between Bi-I and Pb-I cation and anion bonds. Second, as explained by theoretical methods in Walsh's paper, the substitution of a cation with a smaller ionic radius reduces the band gap [41]. When this point of view, the ionic radius of the Pb element is 0.132 nm, while the ionic radius of the Bi element is 0.117 nm. Thus, the use of a smaller cation (Bi instead of Pb) will reduce the band gap of the crystal phase. Our work has shown that the effect of the reduction of the cation size on the band gap is more dominant than the influence of the change in the antibonding character of the bonds. As a result of this effect, the band gap of the $CH_3NH_3BiI_3$ material is considerably reduced when compared to $CH_3NH_3PbI_3$. However, the calculated band gap of 0.2738 eV is not the ideal band gap for a photoabsorber. The band gap of the $CH_3NH_3BiI_3$ crystal form is very poor in terms of usability in solar cells. Furthermore, the band gaps of the non-stoichiometric crystal forms described in the following sections yield promising results.

Electronic properties of Non-stoichiometric phases

While investigating the electronic properties of the non-stoichiometric $CH_3NH_3Pb_{(1-x)}Bi_xI_3$ material produced by varying x values from 0.125 to 0.750, the $CH_3NH_3Pb_{0.875}Bi_{0.125}I_3$ crystal structure of were first obtained by with $x = 0.125$. The super cell of this phase is given in Fig. 2a). The electron band distribution of the optimized crystal phase is calculated in the direction of $F \rightarrow R \rightarrow \Gamma \rightarrow M \rightarrow \Gamma \rightarrow F$. In order to increase the resolution, the $R \rightarrow \Gamma \rightarrow M$ symmetry points within the band gap region are zoomed. The electronic band distribution is given in Fig. 4a). The band gap is calculated as 1.3057 eV. While the band gap of the stoichiometric $CH_3NH_3PbI_3$ structure is on the R symmetry point; in the non-stoichiometric $CH_3NH_3Pb_{(1-x)}Bi_xI_3$ forms, the band gap is observed at the Γ symmetry point. As given in Fig. 4a), electronic states under the valence band consist of contributions from Pb atoms in the range of −10 eV to −8 eV. while there is a small contribution from the s, p and d states of Pb atoms in the valence band between −4 eV and 0 eV, especially there are a contribution of the 5 s, 5p states of both I atoms in the valence band between −2 eV and −4 eV, which is not dominant of the contributions of the s, p and d states of both Pb and Bi atoms. Furthermore, the 5 s-p states of the I atoms contributes significantly to the overall distribution of the valence band. The effect of this contribution increases towards the top of valence band. In the conduction bands, while the contributions of Bi atoms is less in the bottom of conduction band, the effect of the Pb atoms increases towards high energy level as relatively (between 1 eV and 2 eV). In addition, the contribution of I atoms is dominant in the level between 1 eV and 4 eV. It has been determined that the addition of Bi^{3+} ions instead of Pb^{2+} ions at $x = 0.125$ ratio to the supercell of the crystal reduces band gap by 22.4%. In Fig. 4b) shows the electronic band and pDOS distribution of the $CH_3NH_3Pb_{0.750}Bi_{0.250}I_3$ crystal form. When the electronic band structure of the phase is examined, it is seen that the contributions from the individual atoms exhibit a similar behavior locally to the crystal structure of $CH_3NH_3Pb_{0.875}Bi_{0.125}I_3$ (x = 0.125). However, especially a distribution of the 6p states of Bi atoms significantly lowers the bottom level of the conduction band. Accordingly, the band gap of the $CH_3NH_3Pb_{0.750}Bi_{0.250}I_3$ crystal structure was calculated to be 0.9254 eV. It has been determined that the $CH_3NH_3Pb_{0.750}Bi_{0.250}I_3$ crystal phase obtained at $x = 0.250$ reduced the band gap value relative to the initial phase by 45%. The calculated band gap values are given in Table 4.

The electronic band and pDOS distribution of the $CH_3NH_3Pb_{0.500}Bi_{0.500}I_3$ and $CH_3NH_3Pb_{0.250}Bi_{0.750}I_3$ crystal phases are given in Fig. 5a) and b), respectively. The band distribution in the two phases exhibits a similar electronic behavior. While the valence band predominantly contains contributions from the I atoms; it is seen in Fig. 5a) and b) that the contributions from the Bi atoms to the lower parts of the conduction band and from the Pb atoms to the middle parts and from the I atoms to the upper part are more visible. The electronic band gaps of both non-stoichiometric phases were calculated to be 1.0863 eV and 1.0895 eV, respectively. The electronic band gap of the phases $CH_3NH_3Pb_{0.500}Bi_{0.500}I_3$ and $CH_3NH_3Pb_{0.250}Bi_{0.750}I_3$ relative to the initial phase was calculated to be about 35% smaller. The combination of Bi^{+3} and Pb^{+2} ions with respect to x ratios in the non-stoichiometric crystal forms provides a mixed contribution of both the antibonding characteristic of Pb-I or Bi-I bonds and the effect of cation size on band gap. As a result of the common contribution of these two effects, the band gap is reduced, but at the efficiency limits it remains at the level of convenience. According to the Shockley Queisser (SQ) limit,

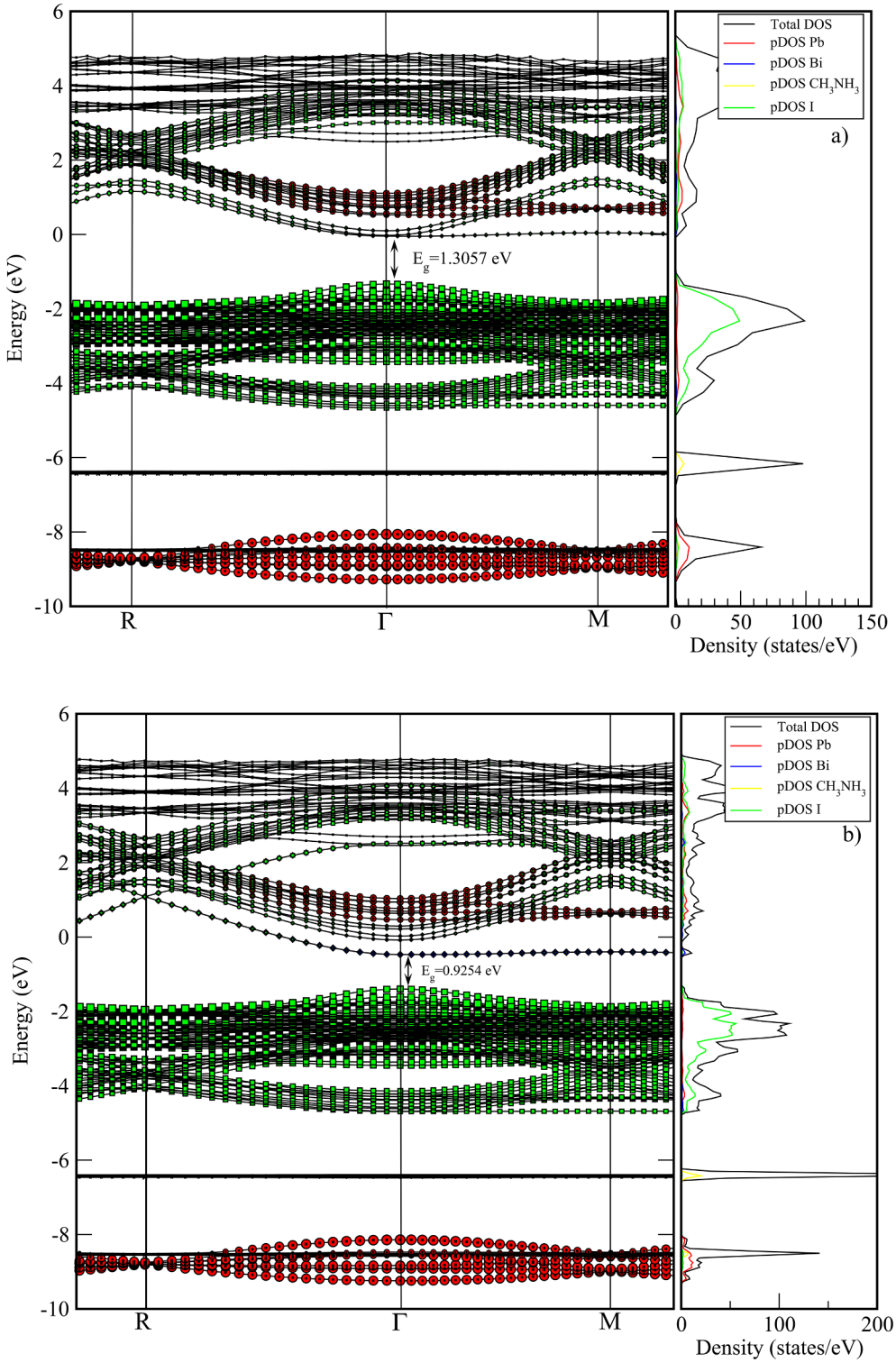

Fig. 4. The calculated band structures of the non-stoichiometric $CH_3NH_3Pb_{(1-x)}Bi_xI_3$ phases designed with ratios a) x = 0.125 and b) x = 0.25 in the direction $F \rightarrow R \rightarrow \Gamma \rightarrow M \rightarrow \Gamma \rightarrow F$. In order to increase the resolution, the $R \rightarrow \Gamma \rightarrow M$ line is zoomed. The fermi level is at 0 eV.

the optimum range for the material to be used is 1.35 eV so that the best efficiency can be obtained from the solar cells [42]. A yield of approximately 33% can be obtained for these band gap values. For this reason, it is important that for effectivity the material have a band gap of around 1–1.5 eV. When we evaluate our results according to the SQ limit, while the $CH_3NH_3PbI_3$ stoichiometric phase remains above the limit with 1.6826 eV band gap, the $CH_3NH_3BiI_3$ phase also remains well below the limit with 0.2738 eV band gap. In the non-stoichiometric phases, it was calculated that the $CH_3NH_3Pb_{0.875}Bi_{0.125}I_3$ crystal structure was the best band gap value. Although the band gaps of the $CH_3NH_3Pb_{0.500}Bi_{0.500}I_3$ and $CH_3NH_3Pb_{0.250}Bi_{0.750}I_3$ phases are within the limits of the SQ, the band gap of the $CH_3NH_3Pb_{0.750}Bi_{0.250}I_3$ phase was found to be below the limit of 1–1.5 eV.

As known, in semiconductor materials, both energy saving and crystal momentum should be maintained in order to ensure the passage of electron through the valence band to the conduction band. The

Table 4
The calculated band gaps of the non-stoichiometric $CH_3NH_3Pb_{(1-x)}Bi_xI_3$ designed by the ratios of x = 0.125, 0.25, 0.50 and 0.75, respectively.

Structures	x ratio	Band gaps
		$E_{band-gap}(eV)$
$CH_3NH_3Pb_{0.875}Bi_{0.125}I_3$	0.125	1.3057
$CH_3NH_3Pb_{0.750}Bi_{0.250}I_3$	0.250	0.9254
$CH_3NH_3Pb_{0.500}Bi_{0.500}I_3$	0.500	1.0863
$CH_3NH_3Pb_{0.250}Bi_{0.750}I_3$	0.750	1.0895

maximum energy state in the valance band and the minimum energy state in the conduction band are each characterized by a certain crystal momentum (k-vector) in the Brillouin zone. If the k-vectors are the same, it is called a direct gap. If they are different, it is called an indirect gap. In cases where there is a direct band transition, the crystal momentum is preserved. In addition, the photons have a very small crystal momentum. Therefore, the values can be taken as zero. The phonons have a higher crystal momentum than photons, although their energy is low. Accordingly, electron transition can be achieved by photon in materials with direct band gap. In materials with indirect band gap, for electron transition, there is a need for a phonon, which the crystal momentum of the phonon equal to the difference between the valence band maximum and the conduction band minimum. That is, while almost all energy in the indirect band transition comes from the photon; all momentum comes from the phonon. In such transitions, since the electrons pass through the intermediate phases, they increase the crystal temperature because they transfer their energies to the crystal lattice. Therefore, the use of material with indirect band gap in optoelectronic devices is unsuitable for efficiency. In optoelectronic devices and sun cells, direct band gap materials with higher optical absorption coefficients and band transition supplied with photon energy should be preferred.***

In the $CH_3NH_3BiI_3$ stoichiometric crystal phase given in Fig. 3b), the contribution from the atoms of Bi at both the Fermi level and the deeper parts of the conduction and valence band is significantly higher than the Pb, CH_3NH_3 and I atoms. As mentioned in the study of Mosconi et al., [8] Bi^{3+} states behave like deep electron trap in Bi-doped perovskite structures. In this respect, while the electronic band gap of the $CH_3NH_3PbI_3$ crystal phase was calculated as 1.6826 eV, the electronic band gap of the $CH_3NH_3BiI_3$ phase obtained as a result of the Bi-doping was calculated as 0.2738 eV. We consider that this decrease in the band range is due to the increase in the potential electron traps of the material as a result of the Bi doping. However, an indirect electronic band transition in the $R \rightarrow M$ direction for the $CH_3NH_3BiI_3$ phase was calculated. In terms of the efficiency of solar cells, $CH_3NH_3BiI_3$ crystal form is not a good material candidate with indirect band transition of 0.2738 eV. In addition, it will not be efficient in terms of its use in optoelectronic devices since it has an indirect band transition. In terms of productivity, perovskite crystal structures show a limited capacity of Bi doping. As given in Fig. 4a), in the $CH_3NH_3Pb_{0.875}Bi_{0.125}I_3$ phase formed by x = 0.125, there are very small contributions from the Bi^{3+} ions, where in the conduction band to the Fermi level and the range of 1–3 eV and in the valence band to the range of −2 eV to −4 eV. Accordingly, the electronic band gap is calculated as 1.3057 eV. At the same time, there is also an electronic direct band transition over the Γ point. In this respect, this phase has a more appropriate band gap for optoelectronic systems. In Fig. 4b), in the $CH_3NH_3Pb_{0.750}Bi_{0.250}I_3$ crystal phase formed by x = 0.250 ratio, the contribution from Bi^{3+} ions to the lowest level of the conduction band is slightly higher than the $CH_3NH_3Pb_{0.875}Bi_{0.125}I_3$ phase. Thus, the electronic band gap was calculated as 0.9254 eV. In this phase, there is a direct band transition through Γ point. Also in Fig. 5a) and b), the electronic band distribution and pDOS of the phases formed by the proportions x = 0.500 and x = 0.750 are given. In these phases, although the contributions from Bi^{3+} ions at the lower levels of the conduction band increased, the band gaps were calculated as 1.0863 and 1.0895 eV, respectively. In both phases, there is a direct band transition through Γ point. Our results of structural and electronic band gap are consistent with experimental and theoretical studies for $CH_3NH_3PbI_3$ stoichiometric crystal phase [1–8,33–38]. However, as far as we know, there is no direct study of structural and electronic band gap for the $CH_3NH_3Pb_{(1-x)}Bi_{(x)}I_3$ non-stoichiometric crystal phases formed at the ratios x = 0.125, 0.5, 0.75 and 1.0.

Conclusion

In this study, the replacement possibility of bismuth with lead atoms located in organic halogen perovskite structure of $CH_3NH_3PbI_3$ was investigated considering the rules of Goldschmidt (GRs), tolerance factor concept (*t*) and Shockley Queisser (SQ) limits by DFT calculations in terms of quantum mechanics. This approach presents an alternative element such as non-toxic metal form of Bismuth element instead of toxic Pb atoms in perovskite solar cell.

The tolerance factor (*t*) for the crystal structure formed as a result of the addition of the Bi^{+3} ion instead of the Pb^{+2} cation was calculated to be 0.85. The 0.85 value indicates that the perovskite is not cubic at room temperature, while obtained crystal structure is very close to the ideal perovskite cubic boundary. This difference between the ionic radius (0.117 nm) of Bi^{3+} and the ionic radius (0.132 nm) of Pb^{2+} is approximately 11.36%. This difference, according to Goldshmidt's empirical substitution rules, is less than 15%, indicating that substitution can occur in complete harmony. In our calculations, it has been determined that the band gap decreases as the conduction band approaches the valence band as a result of the displacement of the Bi^{3+} ion. The reason for this effect is that the difference between electronegativity of Bi, Pb and I elements is rather small. This small difference in electronegativity has little effect on the antibonding character between $Bi-I$ and $Pb-I$ cations and anions. As explained by theoretical methods in Walsh's paper, the substitution of a cation with a smaller ionic radius reduces the band gap. Our work has shown that the effect of the reduction of the cation size on the band gap is more dominant than the influence of the change in the antibonding character of the bonds. As a result of this effect, the band gap of the $CH_3NH_3BiI_3$ material is considerably reduced when compared to $CH_3NH_3PbI_3$. However, the calculated band gap of 0.2738 eV is not the ideal band gap for a photoabsorber. The band gap of the $CH_3NH_3BiI_3$ crystal form is very poor in terms of usability in solar cells. Furthermore, the $CH_3NH_3BiI_3$ crystal form has an indirect band transition ($R \rightarrow M$ direction) and is therefore not an efficient material for optoelectronic systems. Contrary to this, the band gaps of the non-stoichiometric $CH_3NH_3Pb_{(1-x)}Bi_xI_3$ crystal forms are given the yield promising results. When the results are evaluated according to the Shockley Queisser (SQ) limit, the crystal structure of the $CH_3NH_3Pb_{0.875}Bi_{0.125}I_3$ formed with respect to the x = 0.125 ratio was determined to be the most suitable crystal structure to the SQ limit with band gap around 1.30 eV. In addition, it has been determined that the band gaps of the $CH_3NH_3Pb_{0.500}Bi_{0.500}I_3$ and $CH_3NH_3Pb_{0.250}Bi_{0.750}I_3$ phases remain within the SQ limit. However, it have been calculated that the $CH_3NH_3PbI_3$ stoichiometric phase is above the SQ limit with a band gap of 1.6826 eV and the $CH_3NH_3BiI_3$ phase is also well below the SQ limit with a band gap of 0.2738 eV.

Our DFT calculations show that organic halogen perovskite compounds in the non-stoichiometric $CH_3NH_3Pb_{(1-x)}Bi_xI_3$ formed by substitution Bi^{3+} ions instead of Pb^{2+} ions may be more efficient than the

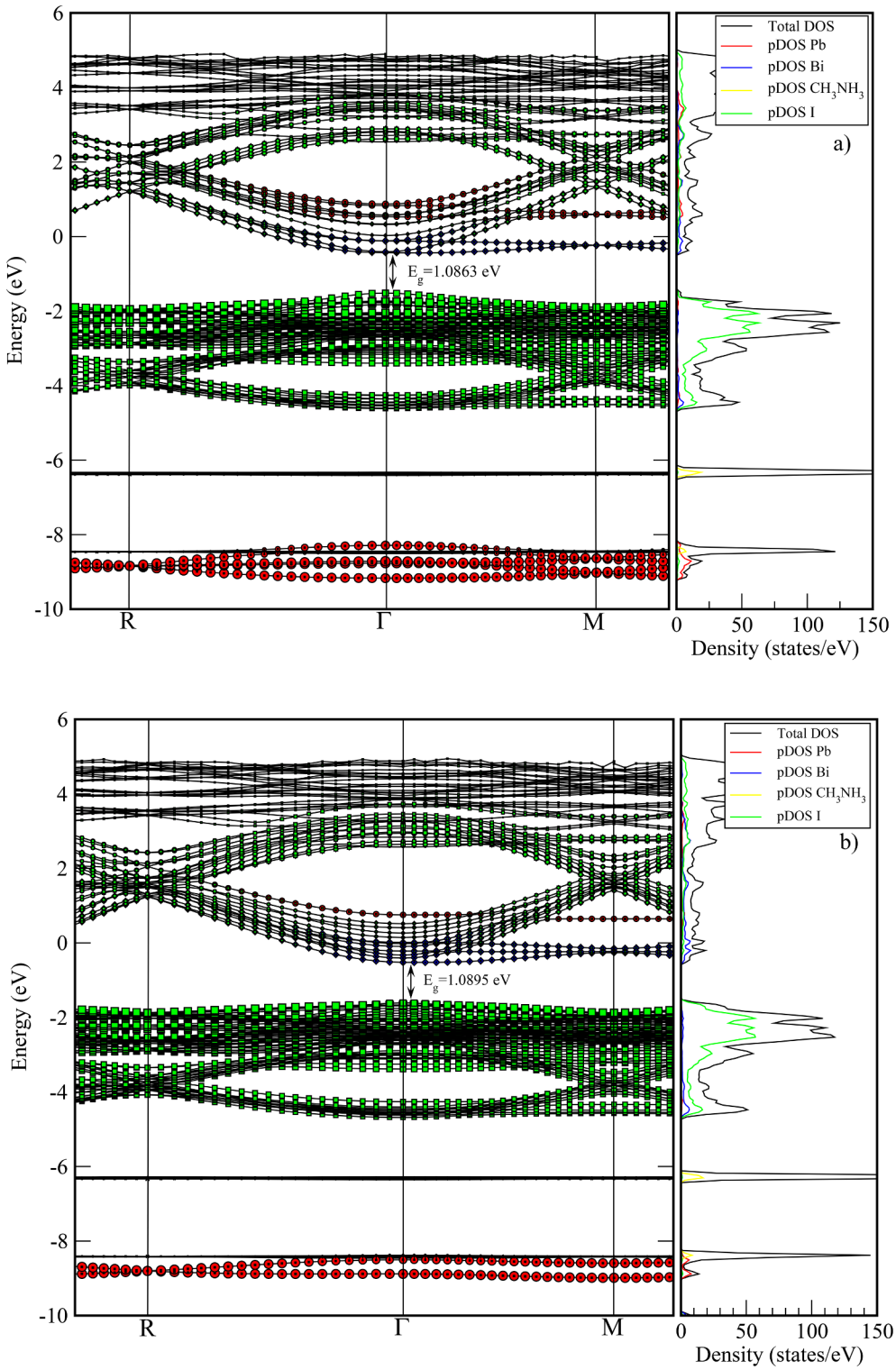

Fig. 5. The calculated band structures of the non-stoichiometric $CH_3NH_3Pb_{(1-x)}Bi_xI_3$ phases designed with ratios a) x = 0.50 and b) x = 0.75 in the direction $F \rightarrow R \rightarrow \Gamma \rightarrow M \rightarrow \Gamma \rightarrow F$. In order to increase the resolution, the $R \rightarrow \Gamma \rightarrow M$ line is zoomed. The fermi level is at 0 eV.

$CH_3NH_3PbI_3$ compounds in terms of environmental safety and solar energy conversion capacity.

Acknowledgements

This work was supported by TUBITAK (The Scientific and Technological Research Council of Turkey) through project number 116F073. Computations are carried out on TUBITAK-ULAKBIM clusters. Authors would like to thank the institution and agency in carrying out this work.

References

[1] Poglitsch A, Weber D. Dynamic disorder in methylammoniumtrihalogenoplumbates (II) observed by millimeter-wave spectroscopy. J Chem Phys 1987;87:6373–8. https://doi.org/10.1063/1.453467.

[2] Rani S, Singh P. First principle study of electronic and optical properties of molecular ion (BF4-) substituted hybrid perovskite (CH3NH3PbI3). AIP Conf Proc 2017;1832:090035https://doi.org/10.1063/1.4980588.

[3] Ando Y, Oku T, Ohishi Y. Rietveld refinement of crystal structure of perovskite CH3NH3(Sb)I3 solar cells, Japan. J Appl Phys 2018;57. 02CE02. 10.7567/JJAP.57.02CE02.

[4] Mosconi E, Amat A, Nazeeruddin MdK, Gratzel M, Angelis FD. First-Principle Modeling of Mixed Halide Organometal Perovskites for Photovoltaic Applications. J Phys Chem C 2013;117:13902–13. https://doi.org/10.1021/jp4048659.

[5] Kojima A, Teshima K, Shirai Y, Miyasaka T. Organometal halide perovskites as visible-light sensitizers for photovoltaic cells. J Am Chem Soc 2009;131:6050–1. https://doi.org/10.1021/ja809598r.

[6] Saffari M, Mohebpour MA, Soleimani HR, Tagani MB. DFT analysis and FDTD simulation of CH3NH3PbI3-xClx mixed halide perovskite solar cells: role of halide mixing and light trapping technique. J Phys D: Appl Phys 2017;50:415501https://doi.org/10.1088/1361-6463/aa83c8.

[7] Jacobsson TJ, Pazoni M, Hagfeldt A, Edvinsson T. Goldschmidt's rules and strontium replacement in lead halogen perovskite solar cells: theory and preliminary experiments on $CH_3NH_3SrI_3$. J Phys Chem C 2015;119:25673–83. https://doi.org/10.1021/acs.jpcc.5b06436.

[8] Mosconi E, Merabet B, Meggiolaro D, Zaoui A, Angelis FD. First-Principles Modeling of Bismuth Doping in the $MAPbI_3$ Perovskite. J Phys Chem C 2018;122:14107–12. https://doi.org/10.1021/acs.jpcc.8b01307.

[9] Goldschmidt VM. Die Gesetze der Krystallochemie. Naturwissenschaften 1926;14:477–85. https://doi.org/10.1007/BF01507527.

[10] McKinnon NK, Reeves DC, Akabas MH. 5-HT3 receptor ion size selectivity is a property of the transmembrane channel, not the cytoplasmic vestibule portals. J Gen Physiol 2011;138:453–66. https://doi.org/10.1085/jgp.201110686.

[11] Shannon RD Revised. Effective ionic radii and systematic studies of interatomic distances in halides and chalcogenides. Acta Cryst A 1976;32:751–67. https://doi.org/10.1107/S0567739476001551.

[12] Hohenberg P, Kohn W. Inhomogeneous electron gas. Phys Rev B 1964;136:864. https://doi.org/10.1103/PhysRev. 136.B864.

[13] Kohn W, Sham LJ. Self-consistent equations including exchange and correlation effects. Phys Rev A 1965;140:1133. https://doi.org/10.1103/PhysRev. 140.A1133.

[14] Kohn W, Becke AD, Parr RG. Density functional theory of electronic structure. J. Phy. Chem. 1996;100. 974. 10.1021/jp960669l.

[15] Kresse G, Furthmuller J. Efficiency of ab-initio total energy calculations for metals and semiconductors using a plane-wave basis set. Com. Mater. Sci. 1996;6:15–50. https://doi.org/10.1016/0927-0256(96)00008-0.

[16] Kresse G, Furthmuller J. Efficient iterative schemes for *ab-initio* total energy calculations using a plane-wave basis set. Phys Rev B 1996;54:11169. https://doi.org/10.1103/PhysRevB.54.11169.

[17] Hafner J. Materials simulations using VASP a quantum perspective to materials science. Commun Phys Commun 2007;177:6–13. https://doi.org/10.1016/j.cpc.2007.02.045.

[18] Kresse G, Hafner J. Ab initio molecular dynamics for liguid metals. Phys Rev B 1993;47:558. https://doi.org/10.1103/PhysRevB.47.558.

[19] Kresse G, Hafner J. Norm-conserving and ultrasokf pseudopotentials for first-row and transition elements. J Phys Condens Matter 1994;6:8245. https://doi.org/10.1088/0953-8984/6/40/015.

[20] Perdew JP, Burke K, Ernzerhof M. Generalized gradient approximation made simple. Phys Rev Lett 1996;77:3865. https://doi.org/10.1103/PhysRevLett. 77.3865.

[21] Methfessel M, Paxton AT. High-precision sampling for Brillouin-zone integration in metals. Phys Rev B 1989;40:3616–21. https://doi.org/10.1103/PhysRevB.40.3616.

[22] Monkhorst HJ, Pack JD. Special points for Brillouin-zone integrations. Phys Rev B 1976;13:5188–92. https://doi.org/10.1103/PhysRevB.13.5188.

[23] Abdelhady AL, Saidaminov MI, Murali B, Adinolfi V, Voznyy O, Katsiev K, et al. Heterovalent dopant incorporation for bandgap and type engineering of perovskite crystals. J Phys Chem Lett 2016;7:295–301. https://doi.org/10.1021/acs.jpclett.5b02681.

[24] Wang R, Zhang X, He J, Ma C, Xu L, Sheng P, et al. Bi^{3+}-doped $CH_3NH_3PbI_3$: red-shifting absorption edge and longer charge carrier lifetime. J Alloy Compd 2017;695:555–60. https://doi.org/10.1016/j.jallcom.2016.11.125.

[25] Hu Y, Bai F, Lui X, Ji Q, Miao X, Qiu T, et al. Bismuth Incorporation Stabilized α-$CsPbI_3$ for Fully Inorganic Perovskite Solar Cells. ACS Energy Lett 2017;2:2219–27. https://doi.org/10.1021/acsenergylett.7b00508.

[26] Zhang Z, Ren L, Yan H, Guo S, Wang S, Wang M, et al. Bandgap narrowing in Bi-doped $CH_3NH_3PbCl_3$ perovskite single crystals and thin films. J Phys Chem C 2017;121:17436–41. https://doi.org/10.1021/acs.jpcc.7b06248.

[27] Zhou Y, Zhou D-D, Liu B-M, Li L-N, Yong Bai Z-J, Xing H, Fang Y-Z, Hou J-S, Sun H-T. Ultrabroad near-infrared photoluminescence from bismuth doped $CsPbI_3$: polaronic defects vs. bismuth active centers. J Mater Chem 2016;4. 2295-2301. 10.1039/C5TC04333F.

[28] Nayak PK, Sendner M, Wenger B, Wang Z, Sharma K, Ramadan AJ, et al. Impact of Bi^{3+} heterovalent doping in organic-inorganic metal halide perovskite crystals. J Am Chem Soc 2018;140:574–7. https://doi.org/10.1021/jacs.7b11125.

[29] Ghosh B, Chakraborty S, Wei H, Guet C, Li S, Mhaisalkar S, et al. Photovoltaic performance of CsBiI: an insight through first principles calculations. J Phys Chem C 2017;121. 17062-17067. 10.1021/acs.jpcc.7b03501.

[30] Calabrese J, Jones NL, Harlow RL, Herron N, Thorn DL, Wang Y. Preparation and characterization of layered lead halide compounds. J Am Chem Soc 1991;113:2328–30. https://doi.org/10.1021/ja00006a076.

[31] Mitzi DB, Wang S, Feild CA, Chess CA, Guloy AM. Conducting layered organic –inorganic halides containing < 110 > -oriented perovskite sheets. Science 1995;267:1473–6. https://doi.org/10.1126/science.267.5203.1473.

[32] Kim HG, Becker OS, Jang JS, Ji SM, Borse PH, Lee SJ. A generic method of visible light sensitization for perovskite-related layered oxides: substitution effect of lead. J Solid State Chem 2006;179:1214–8. https://doi.org/10.1016/j.jssc.2006.01.024.

[33] Tao SX, Cao X, Bobbert PA. Accurate and efficient band gap predictions of metal halide perovskites using the DFT-1/2 method: GW accuracy with DFT expense. Sci Rep 2017;7:14386. https://doi.org/10.1038/s41598-017-14435-4.

[34] Noh JH, Im SH, Heo JH, Mandal TN, Seok SI. Chemical management for colorful, efficient, and stable inorganic-organic hybrid nanostructured solar cells. Nano Lett 2013;13:1764–9. https://doi.org/10.1021/nl400349b.

[35] Dang Y, Tao X, Liu Y, Sun Y, Yuan D, Liu X, et al. Bulk Crystal Growth of Hybrid Perovskite Material CH3NH3PbI3. RSC Pub Cryst Eng Comm 2013;00:1–3. https://doi.org/10.1039/C4CE02106A.

[36] Phuong JQ, Yamada Y, Nagai M, Maruyama N, Wakamiya A, Kanemitsu Y. Free carriers versus excitons in CH3NH3PbI3 perovskite thin films at low temperatures: charge transfer from the orthorhombic phase to the tetragonal phase. J Phys Chem Lett 2016;7(13):2316–21. https://doi.org/10.1021/acs.jpclett.6b00781.

[37] Yamada Y, Nakamura T, Endo M, Wakamiya A, Kanemitsu Y. Near-band-edge optical responses of solution-processed organic-inorganic hybrid perovskite CH3NH3PbI3 on mesoporous TiO2 electrodes. Appl Phys Exp 2014;7:032302https://doi.org/10.7567/APEX.7.032302.

[38] Kim HS, Lee CR, Im JH, Lee KB, Moehl T, Marchioro A, et al. Lead iodide perovskite sensitized all-solid-state submicron thin film mesoscopic solar cell with efficiency exceeding 9%. Sci Rep 2012;2:591. https://doi.org/10.1038/srep00591.

[39] Wang F, Grinberg I, Rappe AM. Band gap engineering strategy via polarization rotation in perovskite ferroelectrics. Appl Phys Lett 2014;104(152903):1–4. https://doi.org/10.1063/1.4871707.

[40] Grote C, Ehrlich B, Berger RF. Tuning the near-gap electronic structure of tin-halide and lead-halide perovskite via changes in atomic layering. Phys Rev B 2014;90(205202):1–7. https://doi.org/10.1103/PhysRevB.90.205202.

[41] Walsh A. Principles of chemical bonding and band gap engineering in hybrid organic-inorganic halide perovskites. J Phys Chem C 2015;119(11):5755–60. https://doi.org/10.1021/jp512420b.

[42] Shockley W, Queisser HJ. Detailed balance limit of efficiency of *p-n* Junction Solar Cells. J Appl Phys 1961;32:510. https://doi.org/10.1063/1.1736034.